Quantitative Analysis of the Grain Morphology in Self-Assembled Hexagonal Lattices

Reinald Hillebrand,* Frank Müller, Kathrin Schwirn, Woo Lee, and Martin Steinhart

Max Planck Institute of Microstructure Physics, Weinberg 2, Halle D-06120, Germany

ABSTRACT We present a methodology for the analysis of the grain morphology of self-ordered hexagonal lattices and for the quantitative comparison of the quality of their grain ordering based on the distances between nearest neighbors and their angular order. Two approaches to grain identification and evaluation are introduced: (i) color coding the relative angular orientation of hexagons containing a central entity and its six nearest neighbors, and (ii) incorporating triangles comprising three nearest neighbors into grains or repelling them from grains based on deviations of the side lengths and the internal angles of the triangles from those of an ideal equilateral triangle. A spreading algorithm with tolerance parameters allows single grains to be identified, which can thus be ranked according to their size. Hence, grain size distributions are accessible. For the practical evaluation of micrographs displaying self-ordered structures, we suggest using the size of the largest identified grain as a quality measure. Quantitative analyses of grain morphologies are key to the systematic and rational optimization of the fabrication of self-assembled materials.

KEYWORDS: self-assembly · nanostructures · quantitative grain analysis · anodic aluminum oxide · image processing

Self-assembled nanostructured materials consisting of discrete entities in a matrix[1] are of tremendous importance in nanoscience and nanotechnology. Examples of such materials are assemblies of nanospheres (colloidal crystals, artificial opals)[2–4] and their inverted structures (inverted opals),[5] block copolymers,[6–8] where the minority component forms hexagonal arrays of spheres or cylinders, block copolymer-derived nanowire arrays,[9] and nanoporous materials containing hexagonal arrays of cylindrical pores. Their grain structure is central to their applicability for a broad range of applications and determines to what extent single entities or whole grains are addressable and to what extent domain scattering deteriorates optical properties of self-assembled materials. However, until now, no methodology has been available that allows analyzing the grain structure quantitatively. Commonly employed 2D Fourier analyses reveal patterns that allow the qualitative identification of the lattice type. Orientation distributions and, to some extent, averaged grain sizes can be obtained by analyzing Fourier patterns. However, the apparent degree of order depends on the size and position of the evaluated area. Furthermore, the evaluation of these patterns is not straightforward and is often hampered by nonoptimal imaging conditions under which the micrographs used for image analysis are obtained. Occasionally, pair distribution functions are used to analyze long-range order. However, they provide an averaged correlation length that does not contain information on the nature of the grains. On one hand, the correlation between the discrete entities may decay within one grain, whereas, on the other hand, correlation may proceed into neighboring grains.

Here we present a methodology for the quantitative analysis of the grain morphology in self-ordered hexagonal lattices. We demonstrate that different hexagonal lattices can be comparatively evaluated and ranked according to the quality of their grain ordering. In particular, distances between nearest neighbors (NNs) and their angular order were used to extract information on the grain structure of hexagonal lattices. For visualization of the grain ordering, scanning electron microscopy (SEM) images were color-coded according to the relative angular orientation of hexagons containing a central entity and its six NNs with respect to a reference direction parallel to the borders of the images. On the basis of NN coordination, the absolute sizes of the grains and grain size distributions were obtained by applying a real-space spreading algorithm. As a practical quality measure for the comparison of the grain ordering in micrographs of self-assembled structures, the size of the largest grain identified is derived and justified. As an

*Address correspondence to hi@mpi-halle.mpg.de.

Received for review October 24, 2007 and accepted April 10, 2008.

Published online May 9, 2008.
10.1021/nn700318v CCC: $40.75

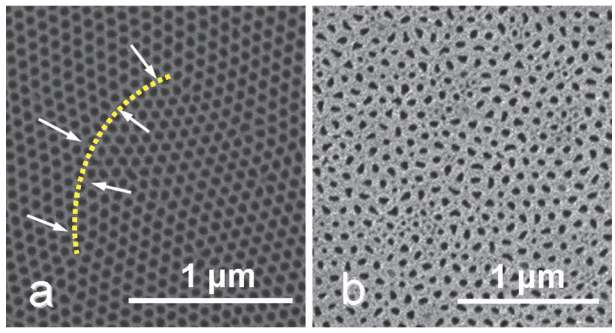

Figure 1. SEM images of nanoporous alumina fabricated by different anodization protocols: (a) mild anodization, missing pores marked by white arrows; (b) hard anodization, disordered pore array.

example in case, the apparent grain morphology in SEM images of self-ordered nanoporous alumina[10–18] was quantitatively analyzed.

Figure 1 shows two examples of self-ordered nanoporous alumina. In Figure 1a, the pore array is well ordered, but some pores are missing, as indicated by the arrows. They may be indicative of a domain wall separating grains with deviating orientation. Figure 1b shows a pore array characterized by more or less random pore sizes and pore shapes and a very poor degree of ordering that can hardly be interpreted in terms of a hexagonal lattice. As an example for quantitative grain analysis, we use an SEM image of nanoporous alumina comparable to that seen in Figure 1a. Figure 2a shows an already thresholded, zoomed-in portion of the micrograph. Depending on the image size and the magnification, the number of pores (*N_pore*) may range from 5000 to 15000. The evaluation of the degree of self-ordering is based on the nearest-neighbor distances, NN_distance, (d_i) and the angles between three nearest neighbors, NN_angle, (α_i) which allow quantifying deviations from the perfect equilateral lattice.

Grain Analysis by Color Coding. The concept of color coding is based on the assumption that the transition between adjacent grains is associated with distinct rotations of the basic six-fold motif of the pore lattice containing a central pore and six NNs. For all lattice sites with correct defect-free six-fold symmetry (6 NN),

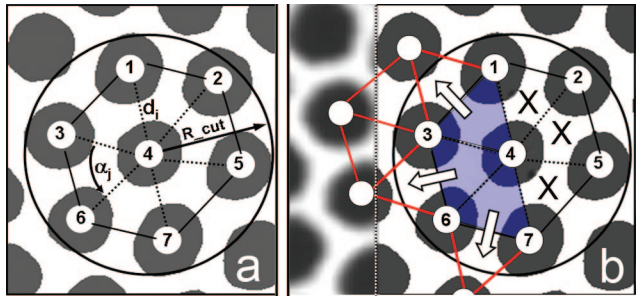

Figure 2. Thresholded and zoomed-in cutout of an SEM image of porous alumina. (a) Definition of the variables NN_distance d_i, NN_angle α_i, and cutoff radius *R_cut*. (b) Scheme introducing the quality evaluation of the pore triangles as well as the strategy of the spreading algorithm. The triangles with an "X" on the right do not fulfill the tolerance criteria. The white arrows symbolize the spread.

TABLE 1. Indexing *i1*, *i2*, and *i3* of the Pores in Figure 2 and the Calculated Values of *Dev_d* and *Dev_*α That Quantify the Quality of the Related Triangles

i	*i1*	*i2*	*i3*	*Dev_d* (%)	*Dev_*α (%)
1	1	3	4	5.2	8.3
2	1	4	2	7.3	11.7
3	2	4	5	7.0	11.0
4	3	6	4	5.0	7.9
5	4	6	7	6.6	10.2
6	4	7	5	8.4	13.6

hexagons within one grain exhibit the same relative angular orientation with respect to a reference direction parallel to the borders of the image. However, to account for the occurrence of distorted hexagons in real lattices, deviations from the ideal hexagonal symmetry have to be considered. To this end, the angles between the lines connecting the central pore and each of its six NNs and the reference direction are determined according to eq 2 in the Methods section. These angles are then, by adding or subtracting multiples of 60°, reduced into a basic angle interval of [−30°, 30°] about the reference direction. Thus, six reduced angles are obtained, the average of which (*6 NN*)*_angle* was calculated as a measure of the relative angular orientation of the hexagon. Areas with the same color (*cf.* Figures 3, 5, 7, and 9) consist of hexagons with the same (*6 NN*)*_angle* value. The same color (red) was assigned to (*6 NN*)*_angle* values of −30° and +30° to account for the 60° rotational lattice symmetry. If a specific pore does not exhibit hexagonal coordination, it is displayed as a white spot to improve the perceptibility of defects located between adjacent grains.

Grain Analysis by a Spreading Algorithm. For grain analysis by a spreading algorithm, the data set of the central coordinates of the pores was combined to triangle coordinates representing triangles of three NNs. In this context, it is important to refer to a crystallographic argument: A two-dimensional hexagonal lattice of *N_pore* pores will provide $N\_tri = 2 \times N\_pore$ triangles containing 3 NNs if there are no defects and if boundary effects are neglected. The structural transition between neighboring grains is accompanied by deviations from the perfect equilateral lattice, *e.g.*, structural defects or missing pores. These lattice deviations are calculated for each of the pore triangles. In particular, the standard deviations of their three side lengths and of their three internal angles, as suggested by Mátéfi-Tempfli et al.,[19] will be used as a measure of the quality of the lattice. Alternative quantities considered for the evaluation of the triangles were less convenient to apply or less sensitive. In the way described in the Methods section, images of nanoporous alumina (see for example Figure 2) are transformed into data sets consisting of triangle indices (*i1*, *i2*, *i3*) and the related deviation values Dev_d_i and Dev_α_i. The deviations of

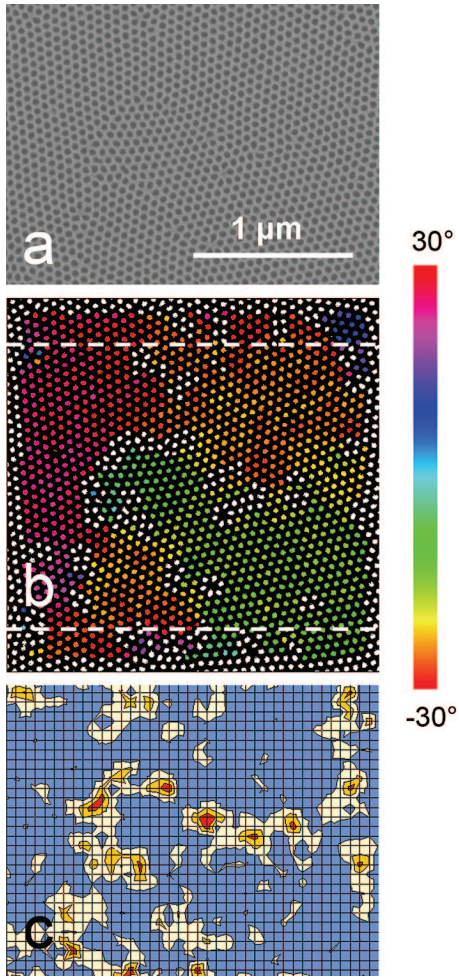

Figure 3. SEM image of nanoporous alumina (U = 25 V, 0.3 M H_2SO_4, t = 1440 min). (a) Cutout of the gray-scale raw image. (b) Pores color-coded on the basis of the *(6 NN)_angle* average relative to the central pore. Pores that have no apparent hexagonal coordination are marked white. (c) Distribution *Dev_*α_i is "flooded" up to *Tol_*α = 9%. Areas that were assigned to be domains (*Dev_*α_i < 9%) appear blue, independent of their orientation.

each triangle from the perfect equilateral triangle are quantified by eqs 3 and 4 (*cf.* Methods section).

Small values of *Dev_*d_i and *Dev_*α_i indicate a locally high perfection of the hexagonal pore lattice with nearly equilateral triangles. A grain is defined as a contiguous ensemble of pore triangles with high ordering, surrounded by distorted ranges. Practically, the introduction of the tolerance parameters *Tol_d* and *Tol_*α allows us to distinguish between areas with smooth hexagonal order within one grain (*Dev_d,*$\alpha \leq$ *Tol_d,*α) and areas characterized by pronounced disorder, *e.g.*, grain boundaries (*Dev_d,*$\alpha >$ *Tol_d,*α). The appropriate determination of *Tol_d* and *Tol_*α is discussed in general below. Here, we focus on Figure 2b and the related Table 1. To adjust selective conditions for the following discussion, we set *Tol_d* = 6.7% and *Tol_*α = 10.5%. The triangles formed by the pores (1, 4, 2), (2, 4, 5), and (4, 7, 5) do not fulfill these quality requirements and are not accepted inside a grain. They are marked with "X" in Figure 2b and assigned to areas separating adjacent grains. The three shaded pore triangles in Figure 2b are within the set tolerances. Therefore, they represent sites from which further grain growth can start, as indicated by the white arrows. The spreading algorithm evaluates whether the new triangles (Figure 2b, left) will expand the grain by sharing two corners with one of the already incorporated triangles. In addition, each new triangle has to fulfill the quality criterion of eq 5a (Methods).

RESULTS AND DISCUSSION

At the beginning of this section, a nanoporous alumina sample (Figure 3) will be analyzed in detail. A careful examination of the cutout of the raw image shown in Figure 3a reveals that several ordered but twisted sub-regions exist. Figure 3b is color-coded as described above. The assigned pore colors represent the mean angle to the six nearest neighbors, *i.e.*, the (*6NN*)*_angle* average (*cf.* color bar: [−30°, 30°]). Pores that do not possess a six-fold neighborhood are marked white. Lattice rotations between the major grains can clearly be recognized by a transition from red to green. The visualization of the local lattice ordering will help to understand the method introduced in Figure 3c.

Figure 3c illustrates the essential steps of the spreading algorithm. The initial square image (512 × 512 pixels) contains 1636 pores, which are transformed into a data set of 3056 triangles, as described above, with the format *i1*, *i2*, *i3*, *Dev_*d_i (%), *Dev_*α_i (%). The $x-y$ coordinates required for each *Dev_*α_i are the centers of the corresponding triangles. The constant blue background in Figure 3c represents the tolerance level, which is assumed to be *Tol_*α = 9% for the graph. The triangles in the blue area were assigned to grains, the others not. As an analogy, one might imagine that a water surface (blue) floods a 3D scenery. For the remaining visible parts of the *Dev_*α_i data in Figure 3c, *Dev_*$\alpha_i >$ *Tol_*α (*cf.* eq 5b). These "rocky" areas of poor lattice quality separate different grains. Their shapes resemble the contours of the white areas in Figure 3b. The blue ranges in Figure 3c cover all triangles fulfilling the tolerance criterion, and contiguous blue areas belong to the same grain. If the water falls, *i.e.*, *Tol_*α is set to a smaller value (*Tol_*$\alpha \downarrow$), the number of grains increases because more mountain ridges subdivide the water area (Figure S1, Supporting Information). If the water level arises, *i.e.*, *Tol_*α increases (*Tol_*$\alpha \uparrow$), the islands are flooded, and the algorithm ends up with one huge grain.

Next, reasonable values for the tolerance parameters have to be identified and applied that provide comparable results for different images. They should be selective and consider the overall ordering of the hexagonal pore lattice. In Figure 4a, the data set representing the pore lattice in Figure 3b is systematically analyzed. The tolerance parameters *Tol_d* and *Tol_*α are

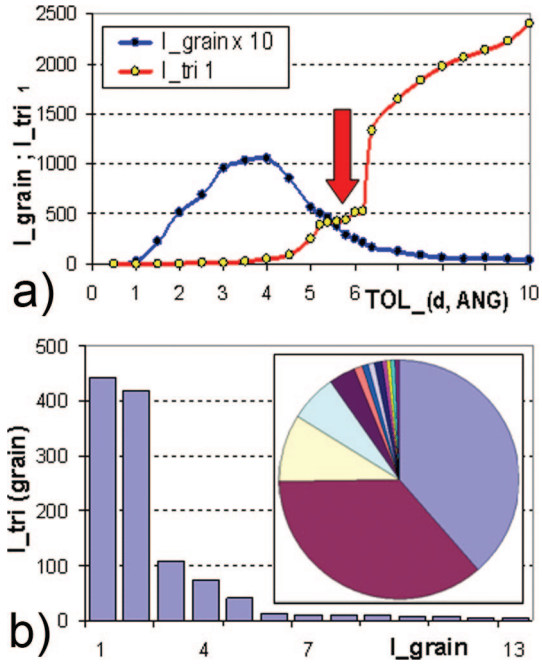

Figure 4. Grain analysis of the SEM image of porous alumina shown in Figure 3. (a) Plot of the number of grains (*l_grain*, blue) and the size of the largest grain (*l_tri*$_1$, red) *vs* the tolerance parameter *Tol*. The quasi-stationary solution is marked by a vertical red arrow (see also Supporting Information). (b) Histogram of the grain sizes *l_tri* (largest grain: 443 triangles) and pie chart of the 13 grains identified for *Tol_d,*α = 5.8%.

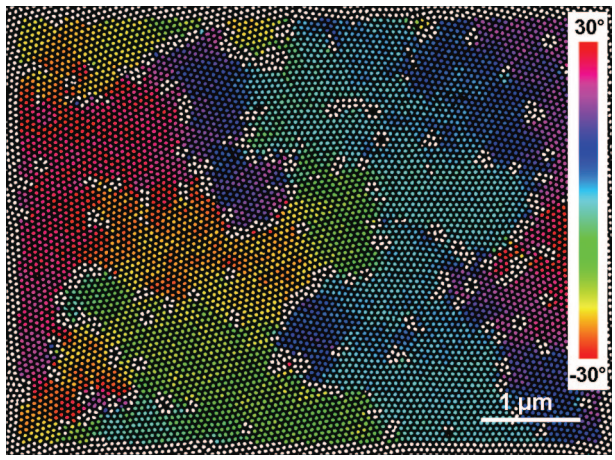

Figure 5. SEM image of porous alumina (*U* = 25 V, 0.3 M H_2SO_4, *t* = 1440 min, mild anodization) containing 7737 pores. The pores are color-coded on the basis of the average of the (6 NN)_angles of the considered pore.

simultaneously varied in the interval *Tol_d,*α = [1%, 10%] with an increment of 0.5%. For very small tolerances, the number of identified grains *l_grain* and the sizes of the largest grains *l_tri*$_1$ are very small; *i.e.*, the criterion is too severe. Depending on the overall ordering, the number of identified grains increases to a maximum at *Tol_d,*α = 4%. Above this value, adjacent grains begin to merge. Further increase of *Tol_d,*α monotonically decreases the number of grains that can be distinguished. Note that there is a conspicuous plateau in the curve representing the size of the largest grain (*l_tri*$_1$) as a function of *Tol_d,*α. Its occurrence indicates relatively stable conditions, identifying the tolerance values of the quasi-stationary solution at *Tol_d,*α = 5.8%, marked by a vertical red arrow (Figure S2, Supporting Information). All other grains then scale with the largest grain in the image if *Tol_d,*α is varied within the range defined by the plateau. This remarkable property turned out to be a general solution criterion, which was recovered in each SEM image of porous alumina analyzed. Going beyond the results reported in ref 19, we suggest a stability criterion for the quasi-stationary solution so that the size determination of the identified grains can be derived. Several other methods of threshold definition were evaluated, *e.g.*, the properties of the overall distribution of *Dev_d*$_i$ (%) and *Dev_*α_i (%), but they were less transparent and were difficult to adapt to extended series of different images. Figure 4b shows the result of the grain analysis of the SEM image seen in Figure 3. The sizes of the grains correspond to the number of contiguous triangles *l_tri* they contain. The histogram shows two large grains with more than 400 triangles. Note that only assemblies of six or more contiguous triangles are regarded as grains. With this assumption, 13 different grains can be identified in Figure 3. The pie chart in Figure 4b shows the portion of the image occupied by specific grains. If the image area analyzed is as small as in this methodical example, boundary effects, *i.e.*, truncated and incomplete grains, may influence the result.

The degree of order of pore arrays in nanoporous alumina depends on parameters such as anodization voltage, electrolyte solution, anodization temperature, and process time. The sample studied here as our first large-scale example was fabricated by mild anodization at a voltage of *U* = 25 V with 0.3 M sulfuric acid solu-

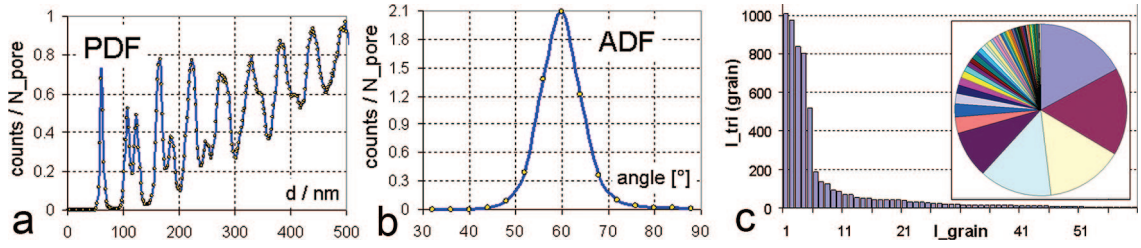

Figure 6. Analysis of the image of porous alumina shown in Figure 5. The PDF (a) and the ADF (b) reveal a high degree of ordering. (c) Histogram of the grain sizes (*l_tri*$_1$ = 1009 triangles, *l_tri*$_1$*/N_pore* = 0.130) and pie chart representing the relative size of the 60 grains identified for *Tol_d,*α = 6.25%.

Figure 7. SEM image of porous alumina (U = 65 V, 0.03 M H_2SO_4, t = 60 min, hard anodization) containing 4393 pores. The pores are color-coded on the basis of the average of the (6 NN)_angles of the considered pore.

tion.[10] Figure 5 shows the color-coded micrograph, where 7737 pores were detected after threshold definition (see also Figure S3, Supporting Information). To prevent edge effects, we only consider pores separated by at least two NN_distances from the image boundary. Grains with uniform *(6 NN)_angle* average are of the same color and easy to recognize, separated by the white dots representing pores with non-hexagonal neighborhood. It is obvious that large grains are truncated at the boundaries of the SEM image (Figure S4, Supporting Information).

Figure 6a,b shows two plots representing the averaged overall ordering of the hexagonal pore lattice seen in Figure 5, namely the pair distribution function (PDF, Figure 6a) and the angular distribution function (ADF, Figure 6b). The curves prove a very high degree of ordering with a pronounced long-range order of the higher-distance shells in the PDF. The narrow ADF is centered around a NN_angle of 60°, as expected for a hexagonal lattice. Note that the grain substructure in Figure 5 results in a Fourier spectrum that exhibits a practically uniform ring pattern representing the nearest neighbors (not shown). Figure 6c summarizes the results of the grain analysis of the SEM image in Figure 5. The histogram of the detected grain sizes shows several large grains containing around 1000 triangles. The pie chart reveals the portion of single grains of the entire area in the image (Figure S5, Supporting Information). With a minimum grain size of six contiguous triangles, 60 different grains could be identified in Figure 5. Roughly spoken, the four largest grains occupy about two-thirds of the area in the image.

The next example selected for grain analysis, porous alumina anodized with 0.03 M H_2SO_4 at a voltage of 65 V for 60 min,[18] contains 4393 pores. A color-coded SEM image of this sample is shown in Figure 7. Monochrome regions, *e.g.*, green or red, and the white contour dots clearly prove the existence of extended subareas in the image with uniform lattice orientation. Figure 8 shows the corresponding PDF (Figure 8a) and ADF (Figure 8b), displaying spatially averaged values of the distance correlation and the angular distribution. Here, the normalized nearest-neighbor peak of the PDF is very sharp but not as high as that seen in Figure 6a. The PDF maxima obtained for increasing distances in the evaluated pore array do not rise and tend to smear out. The ADF is clearly centered around the hexagonal angle of 60°, but the half-width obviously increased as compared to that of the ADF curve shown in Figure 6b. The histogram and the pie chart in Figure 8c present the results of the grain size analysis obtained from Figure 7. As is obvious from the histogram, one grain with a size of 645 triangles clearly dominates the image field. In total, there exist 39 grains that contain more than six contiguous triangles. Moreover, four medium-sized grains ($l\_tri > 100$) and various small and smallest ordered fragments appear in the pie chart.

The third SEM image analyzed in detail represents poorly ordered porous alumina anodized in 0.03 M H_2SO_4 at a voltage of U = 65 V for 15 min. The color-coded image shown in Figure 9 shows many white spots, indicating that the six-fold nearest-neighbor geometry is widely violated. Only in the lower right-hand part of Figure 9 do some small monochromatic areas appear. The data acquisition in the SEM raw image provided the coordinates of 9006 pores. They were used

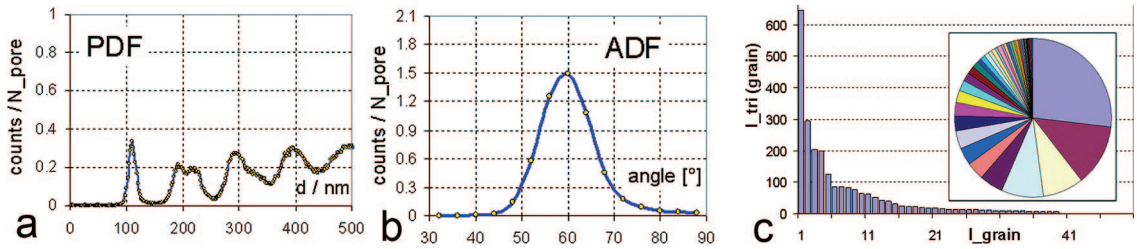

Figure 8. Analysis of the image of porous alumina shown in Figure 7. The PDF (a) shows a decay of the long-range order. The angular coordination ADF of NN_pores (b) indicates that the pores form a hexagonal lattice. (c) Histogram of the grain sizes (l_tri_1 =645 triangles, l_tri_1/N_pore = 0.147) and pie chart representing the relative size of the 39 grains identified for Tol_d,α = 6.88%.

Figure 9. SEM image of porous alumina (U = 65 V, 0.03 M H_2SO_4, t = 15 min, hard anodization) containing 9006 pores. The pores are color-coded on the basis of the average of the (6 NN)_angles of the considered pore.

to calculate the PDF as well as the ADF shown in Figure 10.

For a direct comparison, both functions are scaled in the same manner as those seen in Figures 6 and 8. It is obvious that, in the PDF of Figure 10a, only one sharp peak corresponding to the NN_distance appears. At distances larger than that from the third coordination shell to the central pore, no correlation can be seen. The ADF in Figure 10b shows a broad maximum, indicating the occurrence of pronounced deviations from a perfect hexagonal lattice. In Figure 10c, the results of the grain analysis of Figure 9 are summarized. Consistent with the shapes of the PDF and the ADF, the sizes of the identified grains are very small. The grain histogram reveals that the largest grain contains a total of 47 triangles. Only 48 grains consisting of six or more contiguous triangles as well as 450 items containing less than six valid pore triangles were identified. In addition, the histogram in Figure 10c indicates that the size of the smaller grains (l_tri_2, ..., l_tri_{48}) decays very slowly. The pie chart clearly reveals the splitting of the entire image area into tiny single grains.

The morphology of self-assembled nanostructured materials depends on the fabrication parameters. The examples discussed above contain large perfect grains including more than 1000 pore triangles (Figure 5), as well as only small, hexagonally coordinated areas (Figure 9). For practical reasons, we suggest comparatively evaluating the apparent grain ordering in imaged areas by one of the following quality parameters based on the size of the largest grain identified: (i) the absolute size of the largest grain (l_tri_1); (ii) parameter (i), but normalized to the total number of grains (l_tri_1/N_grain); (iii) parameter (i), but normalized to the total number of pores (l_tri_1/N_pore).

Table 2 shows, for example, the results of the grain analysis of Figures 5, 7, and 9, which clearly rank the level of self-ordering in the hexagonal lattices analyzed. For direct, quantitative comparison of the apparent degree of self-ordering in a series of micrographs, we prefer the absolute size of the largest grains (l_tri_n) identified in each of the images as a feasible quality measure, if the number of discrete entities such as pores is large and comparable. It should be noted that truncations of large grains at the image boundaries may influence the attainable accuracy. It is not our intention to discuss to what extent images recorded by means of various microscopic techniques are representative of the entire sample under investigation. However, the ability of comparing of such images, independent of whether they show one and the same or different samples, appears to be important for the engineering of self-assembly processes.

Figure 11 summarizes the analysis of five nanoporous alumina samples by comparison of their grain morphologies. The anodization voltage was kept constant at U = 65 V, whereas the anodization time t (min) was varied. Figure 11a shows the dependence of the size of the largest grains l_tri_1 on t. It is obvious that the largest grains form for t = 60 min. Figure 11b displays the size distribution of the 10 largest grains in SEM images of each of the five samples evaluated. It is apparent that, in samples containing large grains (t = 30 min to t = 90 min), the largest grain is significantly larger than the second-largest grain, which is in turn significantly larger than the third-largest grain, *etc*. However, the grains identified in these highly ordered samples are still larger than those found for t = 15 min and t = 120 min. The latter samples obviously consist of many small grains of a similar size. It is clearly seen that grain analysis provides information on the morphology of self-ordered

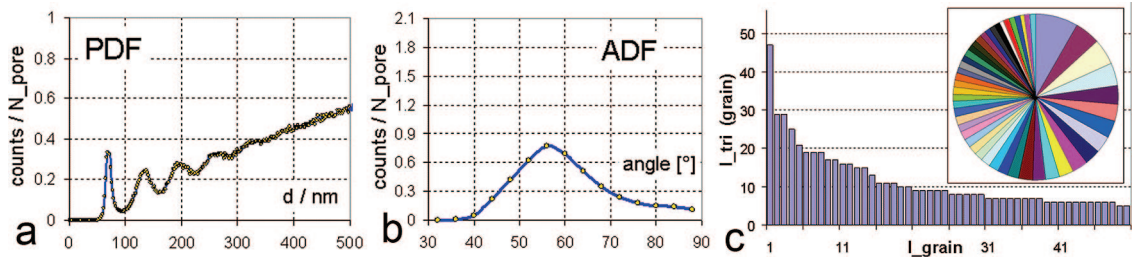

Figure 10. PDF (a) and ADF (b) of Figure 9, proving a poor overall ordering and a poor angular coordination of NNs. (c) Histogram of the grain sizes (l_tri_1 = 47 triangles, l_tri_1/N_pore = 0.0052) and pie chart representing the relative size of the 48 domains identified for Tol_d,α = 7.5%.

TABLE 2. Possible Quality Parameters (Right), Based on the Largest Identified Grains *l_tri*$_1$[a]

image	*N_pore*	*N_grain* (≥6)	*l_tri1*	*l_tri*$_1$/*N_grain*	*l_tri*$_1$/*N_pore*
Figures 5, 6	7737	60	1009	16.82	0.130
Figures 7, 8	4393	39	645	16.54	0.147
Figures 9, 10	9006	48	47	0.979	0.0052

[a]The absolute number of contained triangles *l_tri*$_1$ is normalized in two different ways (*cf.* main text). The numbers characterize the over-all grain distribution and ordering.

nanostructures that goes beyond information accessible from PDFs and ADFs alone.

CONCLUSIONS

A methodology for the analysis of the grain structure in self-assembled hexagonal arrays has been presented. As an example, self-ordered porous alumina was studied, where the degree of self-ordering can be controlled by the anodization parameters. The presented method of grain structure characterization is based on image processing of microscopic images. Thresholding of the digital images yields data sets of the central pore coordinates, which are the input for the calculation of the pair distribution function, the angular distribution function, and the algorithms of lattice order evaluation, *i.e.*, the grain analysis. The grain structure of the hexagonal pore lattice was studied in two ways. For visualization of the overall grain arrangement, a color-coding technique was developed, in which colors were allocated to grains according to the relative angular orientation of their six-fold basic pattern with respect to the image borders. The transition between adjacent grains is indicated by a change in the angular orientation and can be accompanied by the occurrence of entities not incorporated into grains.

In the second approach, the information provided by the microscopic image is transformed into a set of interconnected triangles. Then, for each triangle of neighboring pores, deviations of the actual side lengths and internal angles from those of an equilateral triangle are determined. The structural transition from one grain to another one is necessarily associated with strong deviations from the perfect lattice. A spreading algorithm with tolerance parameters allows for identification of the single grains. Three examples of self-ordered nanoporous alumina exhibiting different morphologies were studied in detail. In addition to the information available from the PDFs and the ADFs, grain analysis reveals the absolute sizes of the grains and grain size distributions, therefore enabling the comparative determination and ranking of the quality of the apparent self-ordering in imaged areas. For practical use, we propose the size of the largest grain identified in the imaged area as a feasible measure of the quality of the grain structure. In general, the rapid evaluation of the grain ordering in hexagonal lattices will enable the optimization of the fabrication of self-assembled materials. Optimizing the addressability of individual entities in the hexagonal lattice requires a well-developed long-range order, *i.e.*, the formation of large grains. The developed methodology is generic and ready to be applied to any self-assembled material forming hexagonal lattices. It may be easily adapted to other lattice geometries, *e.g.*, square lattices, by replacing the triangular basic pattern with a quadratic one. Possible lattice distortions may be evaluated in an analogous way.

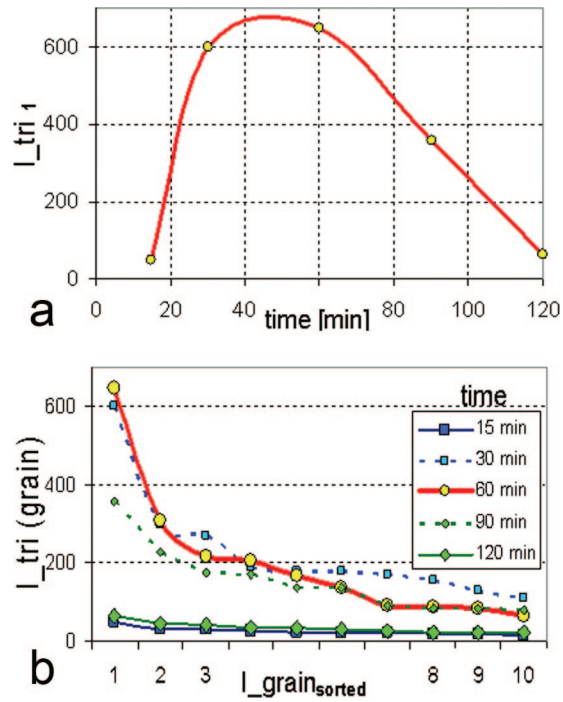

Figure 11. Grain analysis of a series of SEM images of porous alumina fabricated under different conditions (U = 65 V, 0.03 M H_2SO_4, hard anodization, anodization times 15−120 min). (a) Absolute size of the largest grains (*l_tri*$_1$) as a function of the anodization time. (b) Size distribution of the 10 largest grains for each anodization time.

METHODS

Data Acquisition. At first, the digital microscopy images of the self-assembled hexagonal structures are preprocessed and thresholded. Standard image-processing software, *e.g.* ImageJ,[20] provides a data set containing the coordinates of all pores (center of mass). Following the notation of Figure 2a, the coordinates of the central pore are $(x_c,y_c) = (x_4,y_4)$. The NN distances to pore i are determined by

$$d_i = \sqrt{(x_i - x_c)^2 + (y_i - y_c)^2} \quad (1)$$

The cutoff radius *R_cut*, which is needed to determine the angles around the central pore and to define triangles, is set to the minimum between the NN peak and the second-nearest-neighbor peak in the corresponding PDFs. The following trigonometric formula is the basis of the angle calculations:

$$\alpha_i = 180° \cdot \mathbf{atan}[(y_i - y_c)/(x_i - x_c)]/\pi \quad (2)$$

Using a coordinate system in which the image borders define the *x* and *y* axes, the slopes of the lines connecting the centers of the central pore and all pores *i* within *R_cut* are computed (Figure S6, Supporting Information). The periodic properties of the function atan in eq 2 require a quadrant/sign adjustment of the results. Finally, the angles are sorted in ascending order.

Data Analysis. A set of pore triangles is defined, the corners of which are given by the central pore and two adjacent NNs within *R_cut* (see Figure 2). In the same way, sets of triangles are defined around each pore, avoiding doublings. The list of valid triangles is stored as index triples (*i1*, *i2*, *i3*) for the subsequent procedure of numerical grain evaluation (spreading algorithm).

Let us assume that the three pores forming the triangle under consideration are given by (x_{i1},y_{i1}), (x_{i2},y_{i2}), and (x_{i3},y_{i3}). Applying eqs 1 and 2, the corresponding side lengths of the triangle d_{i1}, d_{i2}, and d_{i3} and the internal angles α_{i1}, α_{i2}, and α_{i3} are obtained. The mean values are defined by $d_{mean} = (d_{i1} + d_{i2} + d_{i3})/3$ and $\alpha_{mean} = (\alpha_{i1} + \alpha_{i2} + \alpha_{i3})/3$ (where $\alpha_{mean} = 60°$ for hexagonal lattices). The deviations of each triangle from the perfect equilateral triangle are quantified by eqs 3 and 4:

$$Dev\_d_i\,(\%) = 100 \times \sqrt{[(d_{mean} - d_{i1})^2 + (d_{mean} - d_{i2})^2 + (d_{mean} - d_{i3})^2]/3}\,/\,d_{mean} \quad (3)$$

$$Dev\_\alpha_i\,(\%) = 100 \times \sqrt{[(\alpha_{mean} - \alpha_{i1})^2 + (\alpha_{mean} - \alpha_{i2})^2 + (\alpha_{mean} - \alpha_{i3})^2]/3}\,/\,\alpha_{mean} \quad (4)$$

Practically, the introduction of tolerance parameters *Tol_d* and *Tol_*α allows us to distinguish between smooth lattice ranges within one grain (eq 5a) and those areas characterized by pronounced disorder, *e.g.*, grain boundaries (eq 5b). The conditions read as follow (Figure S7, Supporting Information):

$$Dev\_d_i \le Tol\_d, \qquad Dev\_\alpha_i \le Tol\_\alpha \quad (5a)$$

$$Dev\_d_i > Tol\_d, \qquad Dev\_\alpha_i > Tol\_\alpha \quad (5b)$$

The algorithm described here was executed for SEM images of self-ordered nanoporous alumina, thus analyzing up to 30000 triangles. In the large-scale computations, the "problem size" was reduced by deleting all triangles that did not fulfill the inner-grain quality criterion in advance. The second part of the algorithm checks the geometrical contiguity of the network of remaining triangles by starting, expanding, and completing grains. The computation time *t* is proportional to the square of the number of triangles *N_tri*. The program can be run on standard PCs.

Acknowledgment. Financial support from the German Research Foundation (STE 1127/8-1) is gratefully acknowledged. K.S. thanks the International Max Planck Research School for Science and Technology of Nanostructures for a scholarship. Fruitful discussions with J. Hohlbein on useful measures of ordering are gratefully acknowledged.

Supporting Information Available: Figure S1, a methodical example of color-coding and flooding the pore image with different *Tol_*α values; Figure S2, the criterion for a quasi-stable solution of the flooding/spreading algorithm (determination of the critical *Tol_d*,α); Figures S3−S5, extensive study of the experimental SEM image shown in Figure 5; Figure S6, illustration of the data acquisition as well as the calculation of the interpore distances and angles; Figure S7, graphical definition of the triangles and the quality evaluation of d_i and α_i. This material is available free of charge *via* the Internet at http://pubs.acs.org.

REFERENCES AND NOTES

1. Hoa, M. L. K.; Lu, M. H.; Zhang, Y. Preparation of Porous Materials with Ordered Hole Structure. *Adv. Colloid Interface Sci.* **2006**, *121*, 9–23.
2. Murray, C. B.; Kagan, C. R.; Bawendi, M. G. Self-Organization of CdSe Nanocrystals into 3-Dimensional Quantum Dot Superlattices. *Science* **1995**, *270*, 1335–1338.
3. Murray, C. B.; Kagan, C. R.; Bawendi, M. G. Synthesis and Characterization of Monodisperse Nanocrystals and Close-Packed Nanocrystal Assemblies. *Annu. Rev. Mater. Sci.* **2000**, *30*, 545–610.
4. Pieranski, P. Colloidal Crystals. *Contemp. Phys.* **1983**, *24*, 25–73.
5. Wijnhoven, J.; Vos, W. L. Preparation of Photonic Crystals Made of Air Spheres in Titania. *Science* **1998**, *281*, 802–804.
6. Bates, F. S.; Fredrickson, G. H. Block Copolymer Thermodynamics—Theory and Experiment. *Annu. Rev. Phys. Chem.* **1990**, *41*, 525–557.
7. Castelletto, V.; Hamley, I. W. Morphologies of Block Copolymer Melts. *Curr. Opin. Solid State Mater. Sci.* **2004**, *8*, 426–438.
8. Abetz, V.; Simon, P. F. W. Phase Behavior and Morphologies of Block Copolymers. *Adv. Polym. Sci.* **2005**, *189*, 125–212.
9. Zschech, D.; Kim, D. H.; Milenin, A. P.; Scholz, R.; Hillebrand, R.; Hawker, C. J.; Russell, T. P.; Steinhart, M.; Gösele, U. Ordered Arrays of ⟨100⟩-Oriented Silicon Nanorods by CMOS-Compatible Block Copolymer Lithography. *Nano Lett.* **2007**, *7*, 1516–1520.
10. Masuda, H.; Fukuda, K. Ordered Metal Nanohole Arrays Made by a Two-Step Replication of Honeycomb Structures of Anodic Alumina. *Science* **1995**, *268*, 1466–1468.
11. Masuda, H.; Hasegwa, F.; Ono, S. Self-Ordering of Cell Arrangement of Anodic Porous Alumina Formed in Sulfuric Acid Solution. *J. Electrochem. Soc.* **1997**, *144*, L127–L130.
12. Li, A. P.; Müller, F.; Birner, A.; Nielsch, K.; Gösele, U. Hexagonal Pore Arrays with a 50−420 nm Interpore Distance Formed by Self-Organization in Anodic Alumina. *J. Appl. Phys.* **1998**, *84*, 6023–6026.
13. Chu, S. Z.; Wada, K.; Inoue, S.; Isogai, M.; Yasumori, A. Fabrication of Ideally Ordered Nanoporous Alumina Films and Integrated Alumina Nanotubule Arrays by High-Field Anodization. *Adv. Mater.* **2005**, *17*, 2115–2119.
14. Lee, W.; Ji, R.; Gösele, U.; Nielsch, K. Fast Fabrication of Long-Range Ordered Porous Alumina Membranes by Hard Anodization. *Nat. Mater.* **2006**, *5*, 741–747.
15. Li, F.; Zhang, L.; Metzger, R. M. On the Growth of Highly Ordered Pores in Anodized Aluminum Oxide. *Chem. Mater.* **1998**, *10*, 2470–2480.
16. Masuda, H.; Yada, K.; Osaka, A. Self-Ordering of Cell Configuration of Anodic Porous Alumina with Large-Size Pores in Phosphoric Acid Solution. *Jpn. J. Appl. Phys.* **1998**, *37*, L1340–L1342.
17. Shingubara, S.; Morimoto, K.; Sakaue, H.; Takahagi, T. Self-Organization of a Porous Alumina Nanohole Array Using a Sulfuric/Oxalic Acid Mixture as Electrolyte. *Electrochem. Solid-State Lett.* **2004**, *7*, E15–E17.
18. Schwirn, K.; Lee, W.; Hillebrand, R.; Steinhart, M.; Nielsch, K.; Gösele, U. Self-Ordered Anodic Aluminum Oxide (AAO) Formed by H_2SO_4 Hard Anodization (HA). *ACS Nano* **2008**, *2*, 302–310.
19. Mátéfi-Tempfli, S.; Mátéfi-Tempfli, M.; Piraux, L. Characterization of Nanopores Ordering in Anodic Alumina. *Thin Solid Films* **2008**, *516*, 3735–3740.
20. Rasband, W. *ImageJ*, release 1.36b; NIH: USA, 2006. (public domain, http://rsb.info.nih.gov/ij/).